frontiers | Frontiers in Earth Science

TYPE Original Research
PUBLISHED 06 November 2025
DOI 10.3389/feart.2025.1690397

OPEN ACCESS

EDITED BY
Xiao-Ping Xia,
Chinese Academy of Sciences (CAS), China

REVIEWED BY
Jian Xu,
Chinese Academy of Sciences (CAS), China
Zhongjin Xiang,
Chinese Academy of Geological Sciences (CAGS), China

*CORRESPONDENCE
Massimo Chiaradia,
massimo.chiaradia@unige.ch

RECEIVED 21 August 2025
REVISED 30 September 2025
ACCEPTED 13 October 2025
PUBLISHED 06 November 2025

CITATION
Chiaradia M (2025) Crustal assimilation in arc magmas controlled by overriding plate thickness.
Front. Earth Sci. 13:1690397.
doi: 10.3389/feart.2025.1690397

Crustal assimilation in arc magmas controlled by overriding plate thickness

Massimo Chiaradia*

Department of Earth Sciences, University of Geneva, Geneva, Switzerland

Magmas erupting in arcs range in composition from MgO-rich basalt to MgO-poor rhyolite. This broad compositional range is due to the sequential crystallization and separation of minerals with different chemical compositions from the cooling magma (a process known as fractional crystallization), to mixing between magmas that have undergone different degrees of fractional crystallization, and to the assimilation of rocks, in which high temperatures allow magmas to partially melt and assimilate them. Although the roles of fractional crystallization and mixing in arc magmas have been addressed on a large scale, the role of crustal assimilation has mostly been assessed at local to regional scales and not at the global scale. Using published whole-rock geochemical data on 18 modern arcs of variable crustal thicknesses (~10–~65 km), this study highlights that correlations of elements (MgO and Co), which are the indices of fractional crystallization, with Nd and Sr isotopes, which are the tracers of assimilation, change systematically in magmatic rocks with the crustal thickness of the arc. These correlations indicate the occurrence of assimilation–fractional crystallization (AFC) processes in arcs of different crustal thicknesses. Based on the results of geochemical modeling, the systematics of the correlations between Sr–Nd isotopes and MgO–Co suggest that the rate of crustal assimilation during fractional crystallization of the magmas increases as the thickness of the arc crust becomes greater, which is a consequence of both these processes occurring at deeper and hotter crustal levels in a thick crust compared to a thin crust. In addition, the rocks that are assimilated by arc magmas in increasingly thick arcs are isotopically more evolved, suggesting that the process of crustal growth, refining, and maturation in arcs results from a continuous reworking of previously formed crust through time by subsequent arc magmatic events.

KEYWORDS

arc magmas, fractional crystallization and crustal assimilation, Nd isotopes, Sr isotopes, crust thickness, subduction

1 Introduction

Subduction-related arc magmatism is responsible for cycling of volatile compounds in the Earth (Wallace, 2005), for devastating eruptions (Miller and Wark, 2008), for the largest concentrations of Cu in the Earth's crust (Sillitoe, 2010), and for continental crust formation and growth (Reimink et al., 2023). Arc magmas display a broad variation of major element contents (e.g., MgO from <1 to >10 wt%; SiO_2 from >70 to <50 wt%), with lithologies ranging from basalt/gabbro to rhyolite/granite. The main process responsible for such

a broad range of chemical compositions is fractional crystallization of mantle-derived basaltic melts (Sisson et al., 2005), which occurs within the crust of the overriding plate. Fractional crystallization is eventually accompanied by the assimilation of crustal rocks, their partial melting, and mixing between the products of these processes, contributing in this way to the more or less continuous compositional range of arc magmas (Reubi and Blundy, 2009). Fractional crystallization and magma mixing have been investigated as general processes responsible for the chemical differentiation and heterogeneity of arc magmas (Sisson et al., 2005; Reubi and Blundy, 2009). The assimilation of crustal materials has been investigated and demonstrated to occur at the local scale for single volcanic edifices, provinces, and thick arc segments, especially in the Andes (Alasino et al., 2022; Chiaradia et al., 2011; Davidson et al., 1991; Harmon et al., 1984; James, 1984; James, 1982; James and Murcia, 1984; Mamani et al., 2008). However, to the best of our knowledge, no studies have attempted to investigate the systematics of crustal assimilation in arc magmas at the global scale, encompassing arcs ranging from thin intra-oceanic to thick continental.

In this study, we focus on the magmatic differentiation paths of 18 modern intra-oceanic and continental arcs characterized by significant differences in crust thickness (from ~10 to ~65 km). The relationship between Nd and Sr isotopes with compatible elements that track fractional crystallization (MgO and Co) is used to evaluate crustal contributions during arc magma differentiation. In fact, correlations between Sr or Nd isotope compositions and differentiation indices, such as compatible or incompatible elements, indicate an assimilation–fractional crystallization (AFC) process, in which fractional crystallization and assimilation occur together during the differentiation of parental magma. The data highlight broad correlations of Nd and Sr isotope systematics of the arcs with their crustal thickness, suggesting a first-order process by which increasing crustal thickness results in progressively higher rates of crustal assimilation accompanying magma differentiation. Additionally, the data suggest that the assimilated material in arcs becomes isotopically more evolved as the arc thickness increases, supporting views of crustal growth and maturation through reworking of previous arc building stages (Belousova et al., 2010; Dhuime et al., 2015).

2 Materials and methods

2.1 Data selection and treatment

Geochemical data on volcanic rocks from 18 arcs (South Sandwich, Mariana, Kermadec, Kurile, Izu–Bonin, New Britain, Lesser Antilles, New Hebrides, Tonga, Kamchatka, Solomon, Central America, Honshu, Mexico, Cascades, Northern Volcanic Zone, Central Volcanic Zone, and Southern Volcanic Zone) with varying crustal thicknesses were initially retrieved from the GEOROC database (https://georoc.eu/) in August 2024 and were filtered to include only samples younger than Mio–Pliocene age and those with minimal alteration (see Filtering criteria in Supplementary Dataset S1). Details on the estimates of crustal thickness, based on geophysical data and models from previous studies, are reported in the explanatory worksheet of Supplementary Dataset S2. The crust types on which the investigated arcs developed range in composition from basalt-dominated oceanic crust (e.g., South Sandwich, Mariana, and Kermadec) to heterogeneous continental crust composed of both mafic and felsic lithologies of various ages (e.g., Mexico, Cascades, Northern Volcanic Zone, Central Volcanic Zone, and Southern Volcanic Zone), passing through crust of intermediate type between these two end-members (e.g., Kamchatka and Central America). The Southern Volcanic Zone (SVZ), retrieved from GEOROC, was subdivided into two segments (northern NSVZ and southern SSVZ) due to a systematic decrease in crust thickness from north to south along this arc (Tassara and Echaurren, 2012), with latitude 37°S chosen as the limit between the two arc segments. For the Northern Volcanic Zone (NVZ), the discussion was limited to the Ecuador segment of the NVZ because it has the largest number of samples of the NVZ with isotope data and a well-characterized crustal thickness (Koch et al., 2021). The Ecuadorian arc is a broad arc that develops upon largely different basement lithologies, ranging from oceanic plateau in the Western Cordillera to the continental crust in the Eastern Cordillera. For this reason, the initial data on Ecuador, retrieved from GEOROC as NVZ, were split into three separate arcs: the Western Cordillera (WNVZ), the Eastern Cordillera (ENVZ), and the Inter-Andean Valley of Ecuador. Due to the low number of samples (N = 38; Supplementary Dataset S1), the Inter-Andean Valley was not considered further. Therefore, at the end of the selection process, data for 20 arc segments (South Sandwich, Mariana, Kermadec, Kurile, Izu–Bonin, New Britain, Lesser Antilles, New Hebrides, Tonga, Kamchatka, Solomon, Central America, Honshu, Mexico, Cascades, Western Ecuador WNVZ, Eastern Ecuador ENVZ, Central Volcanic Zone, Northern Southern Volcanic Zone NSVZ, and Southern Southern Volcanic Zone SSVZ) were available (Supplementary Dataset S1).

Rocks classified as alkaline in the GEOROC database and rocks with MgO contents higher than 12 wt% were excluded from the final dataset because they may represent peculiar processes in the back-arc (e.g., shoshonitic rocks of the Ecuadorian back-arc) or cumulates. The remaining samples were placed with their available coordinates into Google Earth Pro to evaluate their positions with respect to the arc axis. Samples that fell significantly outside the arc axis (e.g., fore-arc, trench, and back-arc) or that represented clusters geographically separated from the bulk of the samples defining the main axis were also excluded (see Filtering criteria and maps for each arc in Supplementary Material). The Nd and Sr isotopic compositions of the samples filtered according to the above criteria for each arc were subsequently submitted to a conservative outlier test based on quantiles above 0.99 and below 0.01. At this point, the samples were also plotted against the latitude and longitude to check for possible systematic changes that could correspond to changes in the mantle source or in the crust along the arc axis (see Filtering criteria in Supplementary Material). All 20 arc segments, except for three (Lesser Antilles, New Hebrides, and Tonga), did not display major systematic changes in Nd and Sr isotope compositions along the arc axis, suggesting that isotope systematics inferred below are a reflection of the entire arc segments considered and are not biased by specific arc portions. The three arcs that did show evident along-arc isotope changes were not considered further because their isotope systematics are evidently biased by along-arc isotope changes in the crust or in the mantle. Two of these arcs,

Lesser Antilles and New Hebrides, were developed upon oceanic crust close to continents, which may supply isotopically evolved material to the arc region. Such a material can be incorporated either at the source through subduction or assimilated at the shallow level, providing a biased signal that is not typical of the majority of arcs developed upon oceanic crust farther away from continents. The third arc, Tonga, interacts in its northern part with a mantle plume, which has influenced along-arc isotope systematics (Ewart et al., 1998). At the end of the filtering process, therefore, 17 of the 20 arcs considered were retained. Additional detailed descriptions of the sample selection criteria for each arc are provided in the Supplementary Material. Although the above three arcs were excluded from the discussion, it is important to highlight that their inclusion would not change the relationships between isotope systematics and crustal thickness discussed below.

To reduce the bias induced by outliers and to extract information on general arc trends, previous studies (Chiaradia, 2014; 2021; Lee and Tang, 2020) have used median values of geochemical parameters for specific bins of a major element, for example, 0.5 wt% bins for MgO. However, in this study, the final dataset for each arc was heterogeneous in terms of the number of samples available with all the needed elemental (MgO and Co) and isotopic ($^{143}Nd/^{144}Nd$ and $^{87}Sr/^{86}Sr$) data. Therefore, for several arcs (South Sandwich, Mariana, Kermadec, New Britain, Solomon, Izu–Bonin, and Central America), instead of using median values, which could be strongly biased because of the reduced number of samples (<5) within some bins, the full sample dataset was used. For the other arcs, median values of geochemical parameters were calculated for 0.5 wt% MgO bins (Supplementary Dataset S1), as in studies by Chiaradia (2014), Chiaradia (2021) and Lee and Tang (2020).

2.2 AFC modeling

Although it may not capture all their complexity, AFC is a reasonable first-order approximation of evolutionary processes in arc magmas (Kemp et al., 2007; Hagen-Peter and Cottle, 2018; Large et al., 2024). AFC is identified by correlations of major and trace elements with radiogenic isotopes, the shape of which depends on the isotopic and element concentration contrasts between the parent magma and the assimilant. The variation in element concentration is controlled both by the fractionation of a specific element between residual melt and crystallizing minerals during the process of fractional crystallization and, to a lesser degree, by the assimilation of crustal material by the magma. However, variations in element concentrations alone are not very diagnostic of assimilation and difficult to quantify in the frame of an AFC process. In contrast, radiogenic isotope variations in a magmatic suite imply an open-system process, and if such variations are systematically correlated with an element (either compatible or incompatible) that is a typical index of crystal fractionation, then AFC is a likely explanation for this correlation. The element concentration highlights (mostly) the crystal fractionation process, whereas the radiogenic isotope variation highlights the concomitant assimilation of an isotopically different material. A trend in which the element concentration variation occurs without concomitant variation in the radiogenic isotope ratio indicates either the lack of assimilation or cryptic assimilation of material that is isotopically similar to the differentiating magma.

To track the occurrence of assimilation during differentiation of arc magmas, MgO and Co were used as the indices of magma differentiation because variations in these two elements typically track fractional crystallization or partial melting processes, whereas Nd and Sr isotopes were used as the indicators of assimilation. The choice of Co among the trace elements displaying a similar behavior to MgO (for all arcs, MgO and Co are positively correlated: Supplementary Dataset S1) was determined by the relatively well-constrainable bulk partition coefficients of this compatible element for modeling purposes. Additionally, because Co is not very chalcophile, sulfide fractionation occurring in thick arcs (Chiaradia, 2014; Jenner, 2017; Lee et al., 2012) does not significantly affect this element as it affects other more chalcophile trace elements (e.g., Ni), making the bulk partition coefficients of the latter more difficult to constrain. Nonetheless, the correlations of $^{143}Nd/^{144}Nd$ and $^{87}Sr/^{86}Sr$ with MgO and Co reported below also hold when several other compatible and incompatible elements are used instead of Co. This is expected because MgO is a universal hallmark of magma differentiation that shows strong (positive or negative) correlations with nearly all major and trace elements.

AFC modeling in the $^{143}Nd/^{144}Nd$–Co and $^{87}Sr/^{86}Sr$–Co space was carried out using the equations provided by DePaolo (1981). In these equations, the r value, that is, the ratio of the mass of the assimilant to the mass of crystallized melt, is a parameter that can provide relative estimates of the thermal state under which assimilation occurs. Values of r close to 0 correspond to pure fractional crystallization; low r-values (<0.3) are typical of low assimilation rates in the upper crust, whereas high r-values (>0.5) are typical of high assimilation rates in the lower crust of thick arcs (DePaolo, 1981).

Because the values of the parameters in the equations provided by DePaolo (1981) may not be unique, they were allowed to vary within geochemically reasonable ranges, as reported in Table 1. The partition coefficient (K_D) value of Nd was allowed to vary randomly between 0.1 and 0.3 (Table 1), due to the generally incompatible behavior of Nd throughout a differentiation process. The K_D of Co, a compatible element, was allowed to vary randomly between 1 and 2.5 (Table 1). Because bulk K_D values of compatible elements may change during differentiation more significantly than those of incompatible elements, depending on fractionating minerals, the impact of such potential change was tested based on the strong correlation of Co with MgO and on the relationship between MgO contents and residual liquid fraction from experiments carried out at mid-crustal pressures (Nandedkar et al., 2014). Indeed, all arcs, independent of their thickness, show the same convex upward Co–MgO trend (Supplementary Dataset S1), which suggests very similar K_D variations independent of crustal thickness. During differentiation, K_D values change with an increase toward the more felsic terms (to allow for the accelerated decrease in Co) but never reach values above 2.5, which justifies the range of values used for Monte Carlo modeling (Table 1).

On the other hand, although element concentrations and isotope compositions of the parental magma of each arc are relatively well constrained by the most primitive terms of each arc, the assimilant is more difficult to constrain. For this reason, a large range of variability was allowed for both element concentrations

TABLE 1 Ranges of values for the parameters used in the equations describing the AFC model.

Parameter	Range for thin arcs	Range for thick arcs	Range for CVZ
Remaining melt	2–100	2–100	2–100
R	0–1	0.05–1	0.05–1
Nd parent (ppm)	5–10	6–11	15–20
Nd assimilant (ppm)	5–45	11–45	15–45
$^{143}Nd/^{144}Nd_{parent}$	0.5129–0.5131	0.51295–0.51297	0.5128–0.5129
$^{143}Nd/^{144}Nd_{assimilant}$	0.5116–0.5132	0.511–0.513	0.5118–0.5129
Co parent (ppm)	60–62	52–55	77–82
Co assimilant (ppm)	60–62	5–40	5–40
K_DNd	0.1–0.3	0.1–0.3	0.1–0.3
K_DCo	1–2.5	1–2.5	1–2.5

Ranges of parent Nd and Co concentrations are from the range of oceanic and continental basalts from the study by Kelemen et al. (2004) and from the data obtained from the GEOROC database (Supplementary Dataset S1). The ranges of Nd and Co concentrations of the assimilant are a larger spectrum of values encompassing mafic to felsic lithologies, also considering the values of the different crustal layers (lower, middle, and upper) described by Rudnick and Gao (2005).

and isotope compositions of the assimilant. The AFC equations were applied for 50′000 (thick arcs and thin arcs) and 2′000′000 (very thick arc of the Andean Central Volcanic Zone, CVZ) initial simulations using a Monte Carlo approach, with a homemade script written in RStudio (R Core Team, 2013) (available from: doi:10.6084/m9.figshare.26030953). The random outputs of the model were then evaluated against the real data to infer the most probable values of the unknown parameters (in particular, $^{143}Nd/^{144}Nd$, $^{87}Sr/^{86}Sr$, Nd, and Co of the assimilant, and the r-value) returned by the model and, therefore, the most likely petrogenetic processes. This was done by keeping only those solutions of the model that reproduced the trends observed in thin (≤20 km), thick (≥30 km), and very thick (~65 km) arcs, using best fit equations and allowing a fixed uncertainty in the parameters of those best fits to retrieve only the successful simulations. The variable numbers of initial simulations (50′000, 50′000, and 2′000′000) were chosen to have, at the end, a similar number of successful simulations reproducing the natural trends (approximately 13′000 each) for thin, thick, and very thick arcs.

3 Results

3.1 AFC trends of the arcs

Median $^{143}Nd/^{144}Nd$ and $^{87}Sr/^{86}Sr$ values of arcs grouped by arc thickness intervals (thin ≤20 km, intermediate ~25–30 km, thick ≥30 km, and very thick 65 km) for bins of 0.5 wt% MgO display distinct evolutionary trends with MgO (Figure 1; see Supplementary Figure S1 for the plots of all individual arcs for $^{143}Nd/^{144}Nd$ and $^{87}Sr/^{86}Sr$ versus MgO and Co). In thin oceanic arcs (South Sandwich, Mariana, Kermadec, Kurile, and Izu–Bonin: average crustal thickness of 16.02 ± 3.4 km), $^{143}Nd/^{144}Nd$ and $^{87}Sr/^{86}Sr$ values display flat trends for decreasing MgO, whereas in increasingly thicker arcs (intermediate, i.e., Kamchatka, Central America, and Honshu: average thickness 27.3 ± 2.4 km; thick, i.e., Mexico, Eastern Ecuador, and Cascades: average thickness 39.7 ± 9.9 km; very thick, i.e., CVZ: thickness of ~65 km), $^{143}Nd/^{144}Nd$ and, to a lesser extent, $^{87}Sr/^{86}Sr$ are shifted consistently to lower and higher values, respectively, and display systematic decreases ($^{143}Nd/^{144}Nd$) or increases ($^{87}Sr/^{86}Sr$) with decreasing MgO. The Nd isotope ratios display a better resolution among arcs with different thicknesses compared to Sr isotopes, for which grouped thin, intermediate, and thick arcs show very little differences and only the very thick CVZ arc stands out compared to the other groups (Figure 1).

These trends are also valid when individual arcs are considered (Supplementary Figure S1). The $^{143}Nd/^{144}Nd$–MgO, $^{143}Nd/^{144}Nd$–Co, $^{87}Sr/^{86}Sr$–MgO, and $^{87}Sr/^{86}Sr$–Co trends for each arc have been approximated by linear correlations to extract statistical parameters, such as regression slopes and intercepts with their associated uncertainties, which allow an easy comparison between Nd and Sr isotope trends, although polynomial correlations yield better correlation coefficients in some cases. Supplementary Dataset S2 reports the slopes, intercepts, and correlation coefficient values of all these linear correlations for the arcs retained, as discussed above, following four different approaches (see below). Supplementary Dataset S2 highlights that the correlation coefficients of the trends of each arc broadly increase with the arc thickness. This is a consequence of the fact that thin arcs display subhorizontal trends in the radiogenic isotope versus element concentration space, which have inherently low correlation coefficients. The increasing values of the correlation coefficients with increasing crustal thickness reflect the establishment of progressively more significant correlations between element and isotope variations due to an increasing isotopic contrast

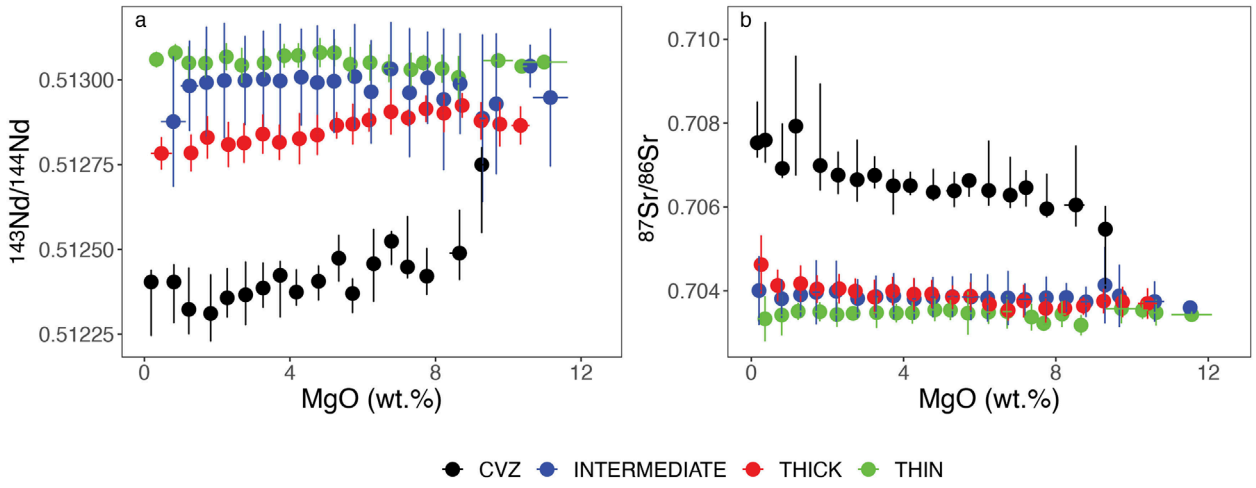

FIGURE 1
Plots of $^{143}Nd/^{144}Nd$ versus MgO **(a)** and $^{87}Sr/^{86}Sr$ versus MgO **(b)** for arc groups of different thicknesses. Each point represents the median values of $^{143}Nd/^{144}Nd$ and $^{87}Sr/^{86}Sr$ for 0.5 wt% intervals of MgO for thin (South Sandwich, Mariana, Kermadec, Kurile, and Izu–Bonin), intermediate (Kamchatka, Central America, and Honshu), and thick (Mexico, Eastern Ecuador, and Cascades) arcs. Very thick arc is represented by the Andean Central Volcanic Zone (CVZ).

between primitive magmatic rocks and assimilant as the crust becomes thicker; this highlights an AFC process. To evaluate the statistical significance of the linear correlations within each arc, four different approaches were adopted (Supplementary Figure S1, Supplementary Datasets S2, S3): 1) correlations based on all points (either as single rock analyses in the arcs with a low number of data points or as median values for 0.5 wt% MgO bins for the arcs with a large number of data points; see above); 2) correlations excluding outliers based on the robust regression approach (Bisquare Weighting method in RStudio); 3) correlations excluding both MgO values > 8.5 wt% and <1.5 wt% but keeping eventual outliers within the 1.5–8.5 wt% MgO interval; 4) correlations excluding both MgO values > 8.5 wt% and <1.5 wt% and also eventual outliers within the 1.5–8.5 wt% MgO interval. Approaches 3 and 4, excluding low and high MgO values, stemmed from the observation that outliers obtained with approach 2 above frequently corresponded to individual samples or bins falling in those extreme ranges (Supplementary Figure S1). There are two main explanations to this. First, bins at the lowest or highest values of MgO for some arcs are calculated on a lower number of samples and may be affected by single rock outliers. Second, rocks in these intervals may correspond to peculiar genetic processes, such as partial melting of portions of the mantle that do not correspond to those producing the main trends between 1.5–8.5 wt% MgO or crustal melting at the low end of MgO (<1.5 wt%) (Hegner and Smith, 1992; Shuto et al., 2006; Takanashi et al., 2012). Nonetheless, it is remarkable that the four different approaches yield linear regressions, slopes, and lower intercepts which are, most of the times, strongly intercorrelated (R > 0.75) and significant (p < 0.0001; Supplementary Dataset S3), if the Western Cordillera of Ecuador (WNVZ) is excluded (see below for this). This suggests that the trends have petrological meaning and are not spurious effects of outliers. For the following discussion, the slopes and intercepts of the regressions obtained with approach 2 (excluding outliers based on the robust regression Bisquare Weighting) are used because considering both isotopic systems, they yield overall higher correlation coefficients than the other approaches (Supplementary Dataset S3). However, as shown in Supplementary Dataset S3, choosing slopes and intercepts obtained with the regressions of the other approaches would not change the conclusions.

Slopes of the best fitting linear trends in the $^{143}Nd/^{144}Nd$–MgO, $^{143}Nd/^{144}Nd$–Co, $^{87}Sr/^{86}Sr$–MgO, and $^{87}Sr/^{86}Sr$–Co spaces correlate significantly with crustal thickness, excluding again the Western Cordillera of Ecuador (Figures 2a,b, 3a,b; see Supplementary Dataset S3 for the full parameters of the linear correlations). These correlations are significant (R = 0.89 for the $^{143}Nd/^{144}Nd$–MgO slope, R = −0.86 for the $^{87}Sr/^{86}Sr$–MgO slope, R = 0.77 for the $^{143}Nd/^{144}Nd$–Co slope, and R = −0.85 for the $^{87}Sr/^{86}Sr$–Co slope, for all p < 0.0001) although exclusion of the Andean Central Volcanic Zone (CVZ), the thickest arc, causes a decrease in both the correlation coefficients and significance (R = 0.69 with p = 0.0045 for the $^{143}Nd/^{144}Nd$–MgO slope; R = 0.57 with p = 0.026 for the $^{143}Nd/^{144}Nd$–Co slope; R = −0.72 with p = 0.002 for the $^{87}Sr/^{86}Sr$–MgO slope; R = −0.68 with p = 0.005 for the $^{87}Sr/^{86}Sr$–Co slope; Supplementary Dataset S3). The $^{143}Nd/^{144}Nd$ and $^{87}Sr/^{86}Sr$ intercept values of the linear regressions at MgO = 0 wt% and Co = 0 ppm, that is, a proxy of, but not necessarily coinciding with (see below), the crustal assimilant, also display more or less significant correlations with crustal thickness (Figures 2c,d, 3c,d). The correlations using the intercept values at MgO = 0 and Co = 0 obtained from the $^{143}Nd/^{144}Nd$–MgO, $^{143}Nd/^{144}Nd$–Co, $^{87}Sr/^{86}Sr$–MgO, and $^{87}Sr/^{86}Sr$–Co slopes including CVZ have R = −0.83 with p < 0.0001, R = −0.90 with p < 0.00001, R = 0.83 with p < 0.0001, and R = 0.84 with p < 0.0001, respectively, whereas, excluding CVZ, the correlations have R = −0.79 with p < 0.001, R = −0.79 with p < 0.001, R = 0.68 with p = 0.0052, and R = −0.70 with p = 0.0038, respectively (Supplementary Dataset S3).

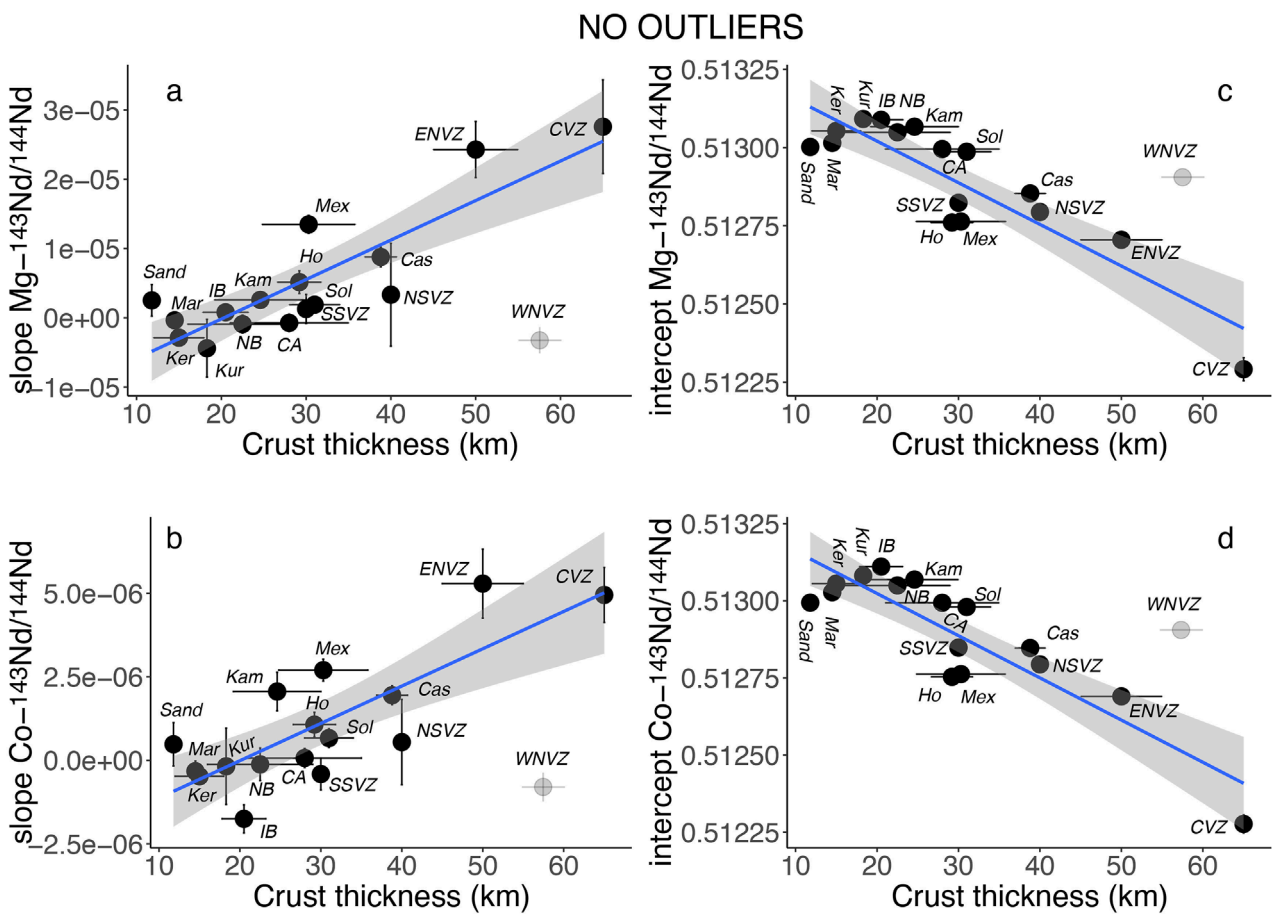

FIGURE 2
Plots of the correlations of crustal thickness with the parameters of the intra-arc correlations of Nd isotopes with MgO and Co. **(a, b)** Correlations of crustal thickness with the slopes of the linear regressions in the $^{143}Nd/^{144}Nd$–MgO and $^{143}Nd/^{144}Nd$–Co spaces, respectively (see Supplementary Figure S1 and Supplementary Datasets S2, S3). **(c, d)** Correlations of crustal thickness with the intercepts of the above correlations at 0 wt% MgO and 0 ppm Co (see Supplementary Figure S1 and Supplementary Datasets S2, S3). Gray envelopes are 1SD uncertainties for the regressions. Abbreviations: Sand, South Sandwich; Mar, Mariana; Ker, Kermadec; Kur, Kurile; IB, Izu–Bonin; NB, New Britain; Kam, Kamchatka; CA, Central America; Ho, Honshu; SSVZ, Southern Southern Volcanic Zone; Mex, Mexico; Sol, Solomon; Cas, Cascades; NSVZ, Northern Southern Volcanic Zone; ENVZ, Eastern Northern Volcanic Zone; WNVZ, Western Northern Volcanic Zone; CVZ, Central Volcanic Zone.

The two sets of intercept values calculated with respect to MgO and Co strongly correlate with each other along slopes of ~1 for both Nd isotopes and Sr isotopes ($^{143}Nd/^{144}Nd_{MgO=0}$ = [0.9800 ± 0.0127]*$^{143}Nd/^{144}Nd_{Co=0}$ + 0.01027 ± 0.0065, R = 0.999; $^{87}Sr/^{86}Sr_{MgO=0}$ = [0.9576 ± 0.0195]*$^{87}Sr/^{86}Sr_{Co=0}$ + 0.0299 ± 0.0137, R = 0.997), which indicates that the $^{143}Nd/^{144}Nd$ and $^{87}Sr/^{86}Sr$ intercept values for each arc are virtually the same using regressions of the Nd and Sr isotopes with either MgO or Co. The depleted mantle (Workman and Hart, 2005) Nd model ages, calculated from the $^{143}Nd/^{144}Nd$ intercept values using the Sm/Nd ratio (0.195) of the bulk continental crust (Rudnick and Gao, 2005), as expected, also show a correlation with crustal thickness and range between ~180 and ~1,470 Ma (Supplementary Dataset S2).

The values of $^{143}Nd/^{144}Nd_{MgO=12}$ and of $^{87}Sr/^{86}Sr_{MgO=12}$ calculated from the regression trends above for 12 wt% MgO, a putative proxy of primary magmas in subduction zones, show less significant linear correlations with crustal thickness (R = 0.74 with p = 0.0012 for Nd isotopes and R = 0.67 with p = 0.0045 for Sr isotopes, including CVZ and excluding WNVZ; Supplementary Dataset S2), which become even less or nonsignificant if CVZ is excluded (R = 0.48 with p = 0.060 for Nd isotopes, R = 0.21 with p = 0.435 for Sr isotopes, excluding WNVZ; Supplementary Dataset S3 and Figure 4).

Overall, the correlations of the Nd isotopes with arc thickness are more significant than those of Sr isotopes, which are more biased by the very thick CVZ arc (Figure 3 and Supplementary Datasets S2, S3). Additionally, the Sr partition coefficient during magmatic differentiation may be very different in thick versus thin arcs (Chiaradia, 2015), due to the dependence of plagioclase stability on pressure, adding complexity to the modeling. In contrast, Nd and Co have more straightforward behaviors during magmatic differentiation (see above). Therefore, the following discussion and modeling focused mainly on Nd isotopes. No correlations between Pb isotope systematics, treated as above for Nd and Sr isotopes, and crustal thickness could be observed.

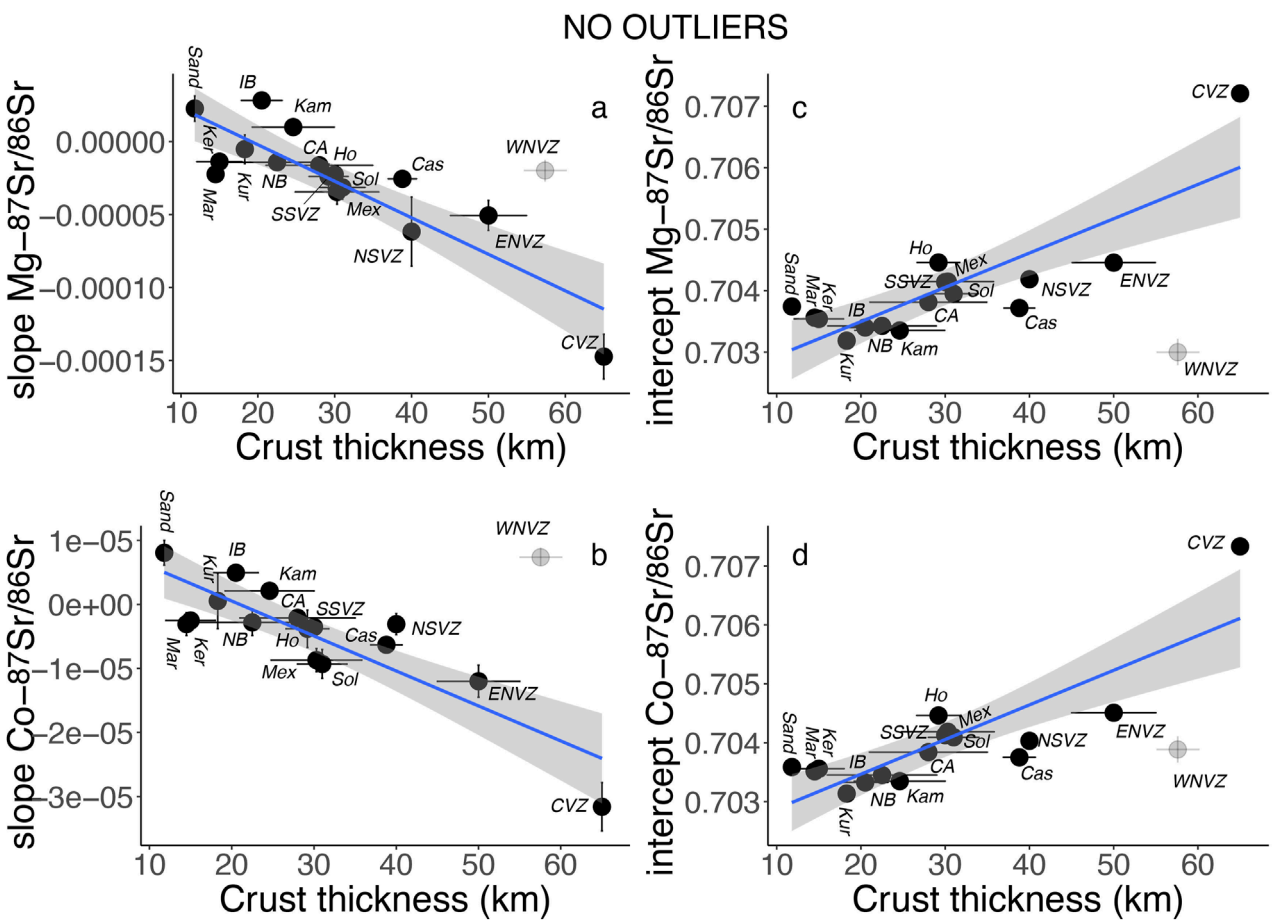

FIGURE 3
Plots of the correlations of crustal thickness with the parameters of the intra-arc correlations of Sr isotopes with MgO and Co. **(a, b)** Correlations of crustal thickness with the slopes of the linear regressions in the $^{87}Sr/^{86}Sr$–MgO and $^{87}Sr/^{86}Sr$–Co spaces, respectively (see Supplementary Figure S1 and Supplementary Datasets S2, S3). **(c, d)** Correlations of crustal thickness with the intercepts of the above correlations at 0 wt% MgO and 0 ppm Co (see Supplementary Figure S1 and Supplementary Datasets S2, S3). Gray envelopes are 1SD uncertainties for the regressions. Abbreviations as in Figure 2.

4 Discussion

Petrographic, geochemical, and isotopic studies indicate that arc magmas are the result of fractional crystallization, recharge of mafic magmas, and assimilation of host rocks or mixing with their partial melts (Sisson et al., 2005; Annen et al., 2006; Reubi and Blundy, 2009) in the so-called transcrustal magmatic or plutonic systems (Cashman et al., 2017; Zellmer et al., 2024). The combined use of isotopic compositions of magmas and incompatible or compatible trace elements, the behavior of which can be modeled through their bulk partition coefficients between crystallizing minerals and residual melt, may provide information on the prevalent magma evolutionary processes occurring in specific volcanic edifices. Such an approach has been widely applied to single volcanic edifices and volcano clusters. On the other hand, although rocks could have different ages, could be sourced from more or less different mantle domains, and could interact with more or less different crustal rocks, the application of such type of modeling to hundreds of km long arc segments may be informative of first-order differences in large-scale processes related to crustal architecture and geodynamic setting, including crustal thickness (Chiaradia, 2014; 2015; 2021; Profeta et al., 2015; Turner and Langmuir, 2015a; 2015b; Zhang et al., 2021; Zhao et al., 2022). In particular, combined similar trends for rocks from spatially and temporally distinct volcanic edifices of the same arc segment may be suggestive of a first-order process occurring in a repetitive spatial and temporal framework for that specific arc segment. To ensure that such trends are not biased by one or few volcanic edifices, along-arc variability of Nd and Sr isotopes was carefully checked, and outliers were excluded (see above and Supplementary Material). Therefore, the general trends described above are likely to be largely the expression of processes encompassing the entire arc segments investigated. Of course, it should be borne in mind that (i) such an approach tends to average out more or less large differences among single volcanic edifices within each arc segment, (ii) the general trends obtained are first-order processes pertinent to those segments, and (iii) single volcanic edifices within each arc may not entirely conform with the general trend of the arc.

Supplementary Figure S1 shows correlations of differentiation indices (e.g., MgO and Co) with Nd ($^{143}Nd/^{144}Nd$) and Sr isotopes ($^{87}Sr/^{86}Sr$) at each arc. These correlations indicate open-system intra-crustal processes relatable to differentiation (e.g.,

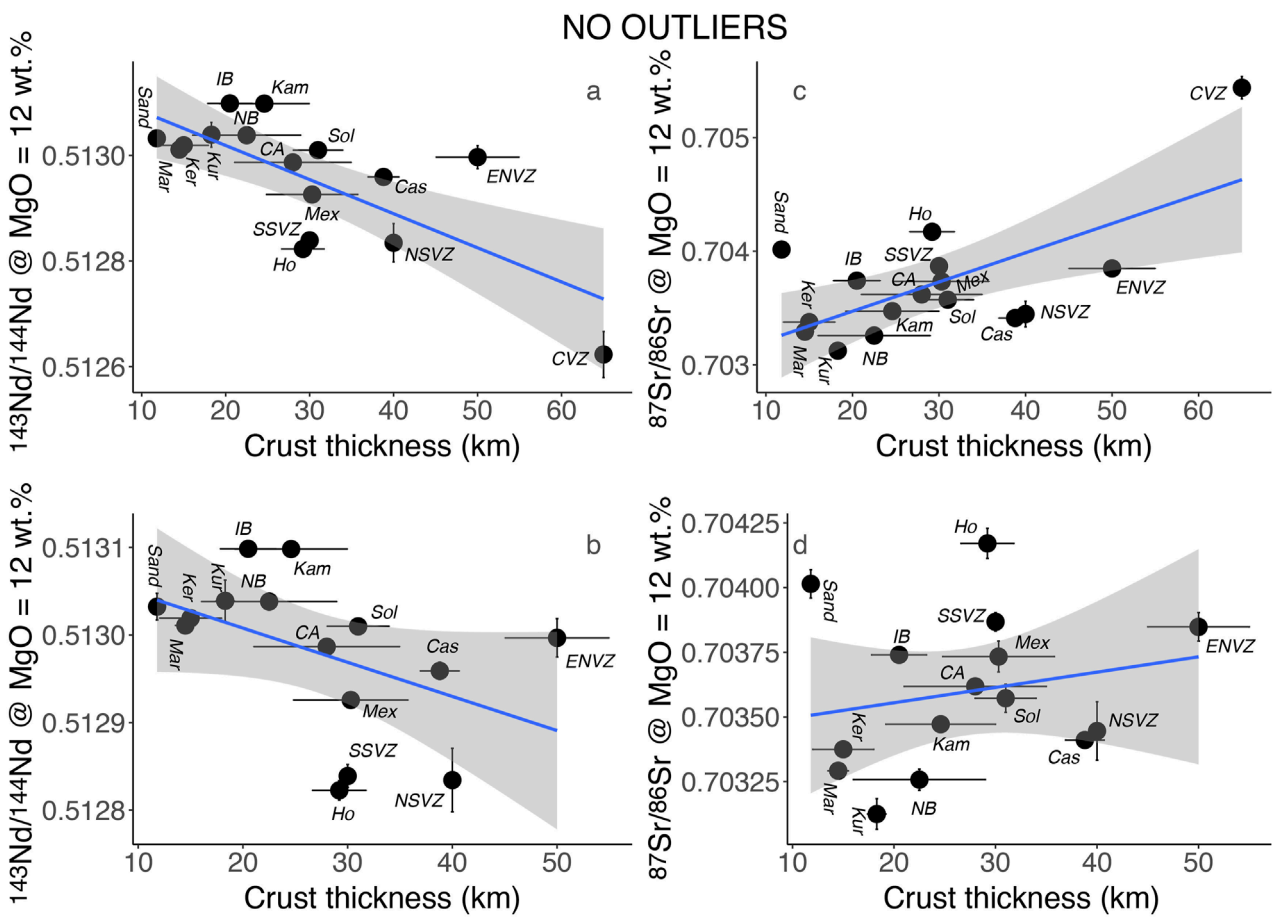

FIGURE 4
Plots of the correlations of crustal thickness with the $^{143}Nd/^{143}Nd$ and $^{87}Sr/^{86}Sr$ values at MgO 12 wt%. **(a)** and **(b)** Correlations of crustal thickness with the $^{143}Nd/^{144}Nd$ and $^{87}Sr/^{86}Sr$ values at MgO 12 wt% for all the arcs. **(c)** and **(d)** Same correlations excluding CVZ. Gray envelopes are 1SD uncertainties for the regressions. Abbreviations as in Figure 2.

fractional crystallization) of a parental magma, accompanied by the assimilation of an isotopically different crustal material. Figures 2a,b, 3a,b show that correlations of $^{143}Nd/^{144}Nd$ and $^{87}Sr/^{86}Sr$ with MgO and Co at each arc have slopes that systematically increase or decrease with the increasing thickness of the arc. The variable slopes of such correlations can be the result of two end-member situations and of any combination thereof: (i) different Nd and Sr isotope values on the high MgO and Co side (parent magma), indicating a source control; (ii) different Nd and Sr isotope values on the low MgO (Co) side (derivative magma), highlighting the role of the crustal assimilant.

The Nd isotope compositions of the putative parental basalts in each arc ($^{143}Nd/^{144}Nd_{MgO=12}$) display a correlation with crust thickness, albeit with a weak statistical significance ($R = 0.74$ and $p = 0.0012$), especially if CVZ is excluded ($R = 0.48$ and $p = 0.060$; Supplementary Dataset S2; Figures 4a,b). In addition, the Sr isotope compositions of the putative parental basalts in each arc ($^{87}Sr/^{86}Sr_{MgO=12}$) show a weak correlation with crust thickness (Supplementary Dataset S2; Figures 4c,d), which is even more biased by the CVZ, as shown by the nonsignificant correlation, if CVZ is excluded ($R = 0.21$ and $p = 0.435$ for Sr isotopes), compared to the correlation when CVZ is included ($R = 0.67$ and $p = 0.0045$). These correlations, although weak, leave open the possibility that the parental basalts could be, at least partly, responsible for the changing slopes of $^{143}Nd/^{144}Nd$ with MgO and Co with arc thickness and will be further discussed below.

In contrast, Figures 2, 3 and Supplementary Dataset S3 show that crustal thickness is more (Nd isotopes) or less (Sr isotopes) significantly correlated with the values of $^{143}Nd/^{144}Nd_{MgO=0}$, $^{143}Nd/^{144}Nd_{Co=0}$, $^{87}Sr/^{86}Sr_{MgO=0}$, and $^{87}Sr/^{86}Sr_{Co=0}$, which are a proxy of the crustal assimilant end-member, both including CVZ ($R = -0.83$ with $p < 0.0001$, $R = -0.90$ with $p < 0.00001$, $R = 0.83$ with $p < 0.0001$, and $R = 0.84$ with $p < 0.0001$, respectively) and excluding it ($R = -0.79$ with $p < 0.001$, $R = -0.79$ with $p < 0.001$, $R = 0.68$ with $p = 0.0052$, and $R = -0.70$ with $p = 0.0038$, respectively). Given the stronger statistical significance of the correlation, this suggests that the crustal assimilant is responsible to a larger extent for the changing slopes of $^{143}Nd/^{144}Nd$ and $^{87}Sr/^{86}Sr$ with MgO and Co with arc thickness.

To better understand the petrological processes behind the systematics shown in Figures 2, 3, the covariations between differentiation of magmas (proxied by Co) and Nd isotopes were

quantified using an AFC process, which, as discussed above, is a realistic and easily modeled simplification of the complex processes of crustal differentiation occurring in arc magmas (Kemp et al., 2007; Hagen-Peter and Cottle, 2018; Large et al., 2024). To evaluate the output of the Monte Carlo-based model of AFC, results have been filtered to fit the natural arc trends in the $^{143}Nd/^{144}Nd$–Co space (see above). Figures 5a–c show the model simulations (blue lines) that best fit to the data available (white circles and squares) for thin arcs (Kermadec and Mariana as examples: Figure 5a), for thick arcs (ENVZ and Cascades as example: Figure 5b), and for the very thick CVZ arc (Figure 5c). The trends with slopes changing for different arc thicknesses in the $^{143}Nd/^{144}Nd$–Co and $^{143}Nd/^{144}Nd$–MgO (but also $^{87}Sr/^{86}Sr$–MgO and $^{87}Sr/^{86}Sr$–Co) spaces suggest that mantle-derived arc basalts differentiating in increasingly thick crust require assimilation of crustal rocks with increasingly lower $^{143}Nd/^{144}Nd$ values (Figures 2, 3, 5a–c).

Figures 5d–f show the two-dimensional density plots returning the most probable combinations of the r parameter and of $^{143}Nd/^{144}Nd_{assimilant}$ (i.e., $^{143}Nd/^{144}Nd_{Mg=0}$ or $^{143}Nd/^{144}Nd_{Co=0}$ for each arc) in successfully reproducing the $^{143}Nd/^{144}Nd$–Co trends of Figures 5a–c. The results of the r parameter for the thin arcs must be considered maximum values because the subhorizontal trends of all these arcs are consistent, in theory, with pure fractional crystallization without any assimilation, a process that cannot be modeled in these plots because not having an assimilant would result in no $^{143}Nd/^{144}Nd_{assimilant}$ values returned by the model and therefore in the impossibility of drawing (Figure 5a).

The results suggest that the most probable combined solutions for the r-values of the AFC process (highest density areas in Figures 5d–f) steadily increase with arc thickness, passing from <0.10 in thin–intermediate arcs to 0.10–0.40 for thick arcs and to ≥0.40 for the very thick CVZ arc. The $^{143}Nd/^{144}Nd_{assimilant}$ value, in contrast, steadily decreases from ~0.5130 through ~0.5123–0.5127 to ~0.5118–0.5123 for thin, thick, and very thick arcs, respectively (Figures 5d–f). Solutions for different assimilation rates (different r-values) of a less radiogenic assimilant (e.g., down to 0.5116 in the simulations) in both thick and very thick arcs are statistically less probable, according to the model (see density contours in Figures 5d–f).

Although the absolute r-values of the model output have to be considered with caution, the model results support the hypothesis that arc magma differentiation in increasingly thicker arcs occurs at average deeper crustal levels (Chiaradia, 2015; Farner and Lee, 2017; Loucks, 2021). This causes the observed increasing assimilation rate of the continental crust (r approaching 1), as a consequence of differentiation processes occurring at deeper and hotter crustal levels in a thick crust than in a thin crust, as described in the MASH (Hildreth and Moorbath, 1988) and hot zone (Annen et al., 2006) processes occurring in the lower crust of thick arcs. The Nd isotopic compositions of the statistically most likely assimilants in thick arcs, according to the AFC model, are more radiogenic than isotopic compositions of basement rocks in those arcs (e.g., basement rocks in the CVZ can have significantly lower $^{143}Nd/^{144}Nd$ values than those corresponding to the model output of Figure 5f). This is also supported by the relatively younger depleted mantle Nd model ages of the crust (Supplementary Dataset S2) compared to known ages of basement rocks in these arc segments and suggests that the assimilated material is not simply basement rock but more likely the roots of the arcs continuously reworked over time by mantle-derived magmas. Overall, this is consistent with assimilation processes occurring in a deep MASH-type zone, in which the basement is continuously refined through interaction (assimilation and homogenization) with mantle-derived basalt during hundreds of millions of years.

Figures 6a–c show the two-dimensional density plots of the most probable Nd and Co concentrations of the assimilant within the ranges chosen for the model (Table 1). The successful simulations for thin arcs (Figure 6a) are consistent with their emplacement upon an oceanic mafic crust characterized by low Nd (≤10 ppm) and high Co (~60 ppm) concentrations. In contrast, the successful simulations for thick arcs (Figure 6b) are consistent with the assimilation of felsic crust characterized by low concentrations of Co (mode at ~10 ppm) and are insensitive to Nd concentrations. Finally, the successful simulations for CVZ (Figure 6c) require assimilation of felsic crust characterized by low Co contents (mode at <10 ppm) and high Nd concentrations (>~20 ppm). The high Nd concentrations are typical of an evolved crust or require mixing with crustal partial melts enriched in an incompatible element, such as Nd, which is consistent with the high r-values returned by the simulations for the CVZ.

As mentioned above, Figure 4 highlights a broad systematic decrease in $^{143}Nd/^{144}Nd$ (and an increase in $^{87}Sr/^{86}Sr$) values at MgO = 12 wt% (i.e., a proxy for primary basaltic arc magmas) as the arc crust becomes thicker. Although the statistical significance of these correlations is weak to very weak if CVZ is excluded (Figure 4), it is worth exploring how crust thickness of the overriding plate might control the Nd (and Sr) isotope variation in primitive arc magmas. This is because although it is broadly accepted that isotopic compositions and incompatible element concentrations and their ratios (e.g., Th/La and Sm/La) in primitive arc magmas are controlled by different types of slab inputs (Elliott et al., 1997; Plank, 2005; Nielsen and Marschall, 2017; Li et al., 2022), plume influence (Ewart et al., 1998; Chiaradia and Fontboté, 2002), and, more generally, ambient mantle composition (Wieser et al., 2019), recent work has highlighted strong correlations of major and trace element geochemistry of primitive arc magmas with crustal thickness (Turner and Langmuir, 2015b; 2015a). Additionally, $^{143}Nd/^{144}Nd_{MgO=12}$ and $^{143}Nd/^{144}Nd_{MgO=0}$ (and $^{87}Sr/^{86}Sr_{MgO=12}$ and $^{87}Sr/^{86}Sr_{MgO=0}$) values correlate with each other ($R = 0.90$ with $p < 0.00001$ for Nd isotopes; $R = 0.92$ with $p < 0.00001$ for Sr isotopes: Figures 7a,b, Supplementary Dataset S2), suggesting that there could be a close relationship between the Nd and Sr isotope compositions of the crustal assimilant and the isotopic composition of the metasomatized mantle wedge. Based on this background, the possibility that Nd (and Sr) isotope compositions of primitive arc basalts also depend on crustal thickness (Figure 4) merits investigation.

A possible mechanism explaining the correlations of Figures 4, 7a,b is the transfer of crustal material into the mantle wedge occurring in such a way to progressively enrich the mantle wedge as the arc thickness increases. In fact, the correlations of Figures 2c,d imply that an increasingly thicker arc crust (the assimilant end-member) has progressively lower $^{143}Nd/^{144}Nd$ values due to the higher contributions of older crust reworked by episodes of younger arc magmatism (Belousova et al., 2010; Dhuime et al., 2015; Farner and Lee, 2017). In its turn, crustal thickness could control arc magma chemistry also at the source through a feedback loop process, in

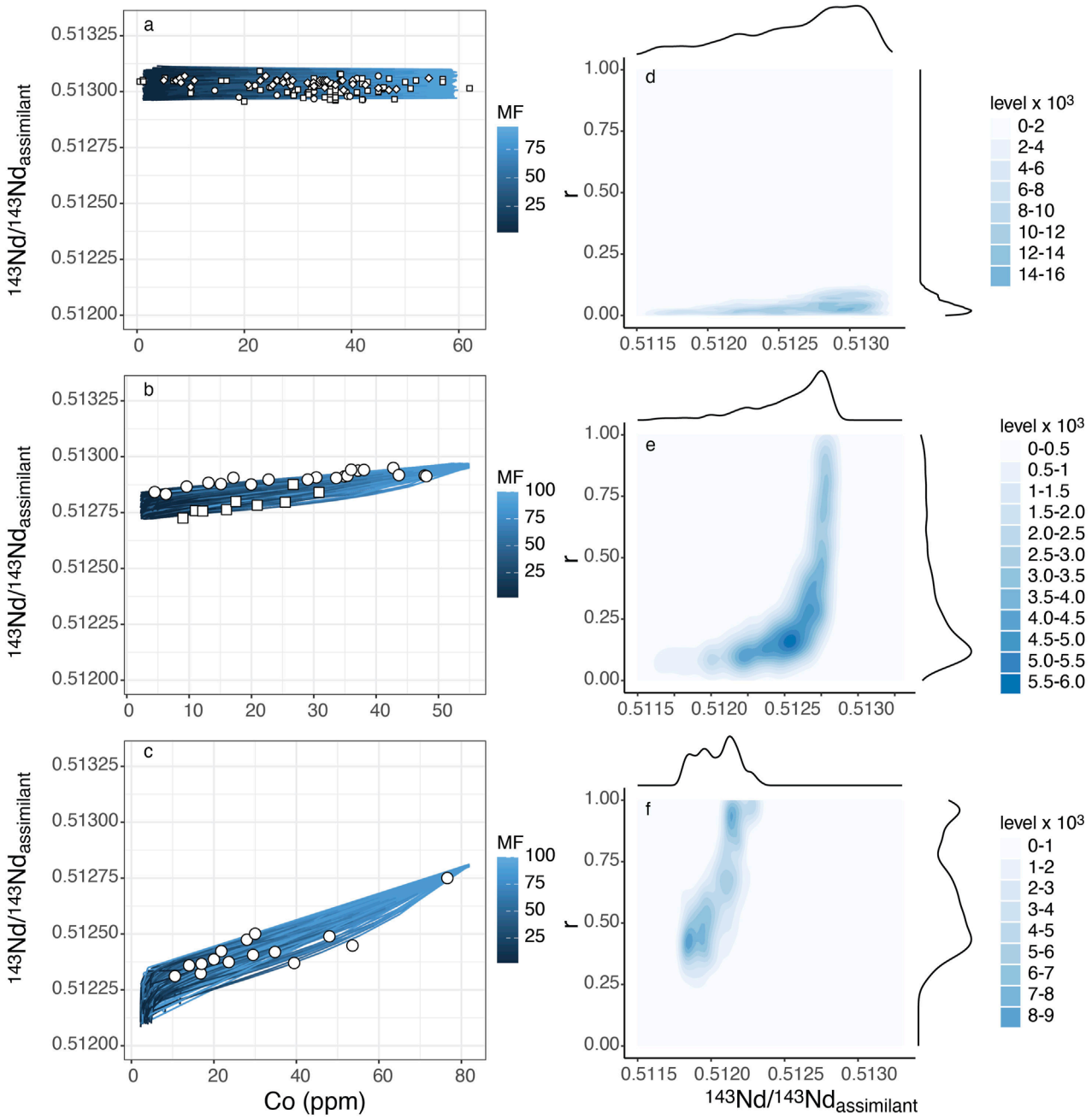

FIGURE 5
Successful simulations of AFC trends reproducing the distribution of thin **(a)** (South Sandwich, Kermadec, and Mariana), thick **(b)** (Cascades = circles and NVZ = squares), and very thick **(c)** (CVZ) arc compositions (median values binned for 0.5 wt% MgO intervals) in the $^{143}Nd/^{144}Nd$ versus Co space. The different shades of blue colors of the AFC trends correspond to different degrees of differentiation (MF = remaining Melt Fraction), as indicated in the plots. Density plots of the successful simulations for thin **(d)**, thick **(e)**, and very thick **(f)** arcs, highlighting the statistically most probable solutions for r values and $^{143}Nd/^{144}Nd$ composition of the assimilant.

which crustal material transfer into the mantle wedge, for example, through subduction erosion (Kay et al., 2005; 2014; Goss and Kay, 2006; Stern, 2011; Jicha and Kay, 2018) or other processes, drives the mantle source of arc magmas to increasingly evolved isotopic compositions (i.e., lower $^{143}Nd/^{144}Nd_{MgO=12}$ and higher $^{87}Sr/^{86}Sr_{MgO=12}$; Figure 4). The mantle-derived arc magmas, during intra-crustal evolution, become increasingly contaminated over time by their interaction with a thicker, older, and more felsic crust, driving it to an even thicker, more felsic, and isotopically evolved crust. The thicker and older the crust the parental arc magmas interact with, the greater the divergence between the parental magmas and the arc crust compared with the earlier, thinner stages of arc crust buildup (Figures 7c,d), highlighting the increasing role of magmatic reworking in crustal growth processes over time.

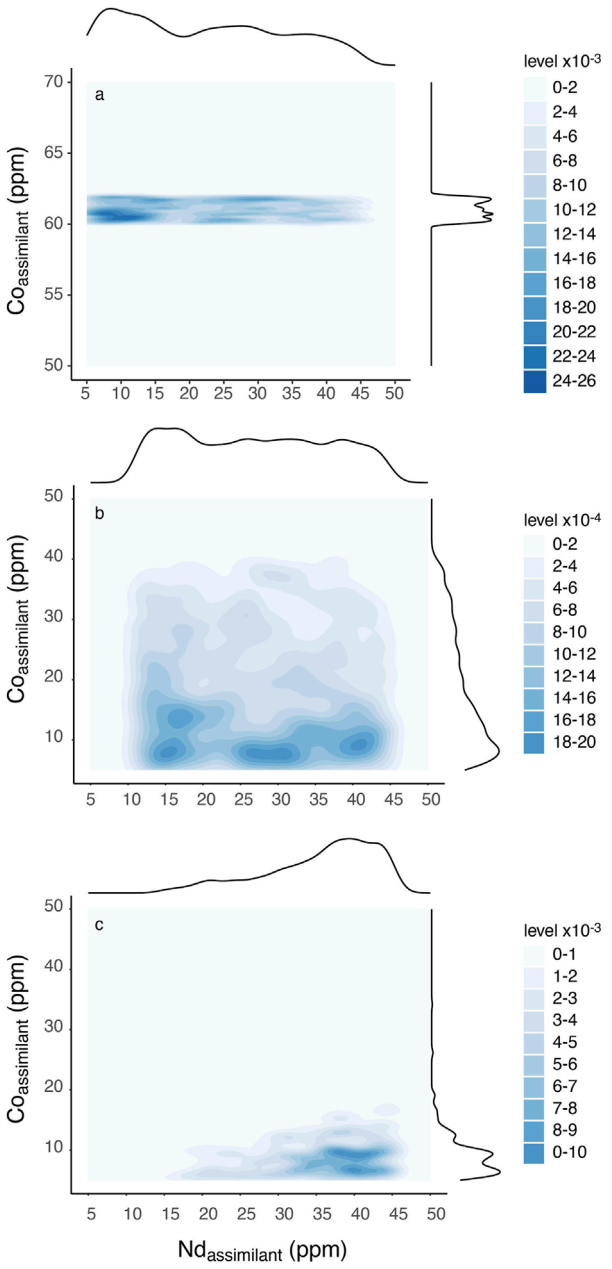

FIGURE 6
Two-dimensional density plots in the Co versus Nd concentrations in the assimilant space **(a–c)** for the successful simulations of thin, thick, and very thick arcs shown in Figure 5.

A notable exception to this trend is the frontal magmatic arc in the Western Cordillera of Ecuador (WNVZ in Figures 2, 3; Supplementary Dataset S1). This magmatic arc is established on a 55- to 60-km-thick crust (Koch et al., 2021), whose roots, however, consist of oceanic plateau mafic rocks, with high-radiogenic Nd and low-radiogenic Sr isotope compositions (Mamberti et al., 2003; Chiaradia, 2009). Therefore, in contrast to the arc established on slightly thinner (45–55 km) crust of the Eastern Cordillera of Ecuador, magmas do not show isotopic evidence of assimilation because of the small isotopic contrast between mantle-derived magmas and mafic assimilant in the lower crust. Subtle correlations between radiogenic isotopes have been, nonetheless, highlighted by previous studies (Chiaradia et al., 2011; 2021; Bellver-Baca et al., 2020), demonstrating that assimilation also occurs in the Western Cordillera of Ecuador, but its quantification remains difficult because of the small isotopic contrast mentioned above. Under this point of view, the Western Cordillera Ecuadorian arc could represent an early stage of ongoing continental crust formation and consolidation, which could be followed by an evolution over time toward an isotopically more evolved lower crust. For the time being, this arc falls off the correlation trends of Figures 2, 3 because it has near 0 slopes despite its large crustal thickness of 55–60 km.

5 Conclusion

In this study, we have investigated the role of crustal assimilation during differentiation of magmas from modern arcs. The dataset used for this investigation was filtered to reduce, as much as possible, the weight of outliers within the investigated arc segments so that the systematics unveiled by this study can be considered the result of first-order processes that occur at the global scale and systematically depend on the crustal thickness of the arcs. Nonetheless, it has to be borne in mind that single volcanic edifices within each arc may not conform to the general trends of the arcs.

In particular, this work has revealed the existence of significant correlations between radiogenic isotope systematics ($^{143}Nd/^{144}Nd$ and $^{87}Sr/^{86}Sr$) of arc magmas and the crustal thickness of 16 magmatic arcs, globally distributed. The data show that the slopes of the linear correlations of Nd and Sr isotopes with differentiation indices (MgO and Co) display systematic changes with the arc crust thickness, which are controlled mostly by the isotopic composition of the crustal assimilant. Such correlations highlight that the AFC process in arc magmas changes systematically with arc thickness. In particular, the assimilation rates of crustal material by arc magmas become higher, and the assimilated crust becomes older in progressively thicker arcs. Although this result may be expected, no previous study has shown this process to occur in such a systematic way at the global scale.

Another relevant point stemming from this analysis is the occurrence of a correlation, albeit weak, of the isotopic compositions of the primitive magmatic end-members (at MgO = 12 wt%) with crustal thickness. This may suggest that the mantle source of arc magmas also exhibits radiogenic isotope compositions that systematically vary with crustal thickness; however, further investigation is needed. For the time being, an explanation to the possible correlation between isotopic compositions of the primitive magmatic end-members and crustal thickness could be increasing subduction erosion of the lower portion of the overriding plate crust as the latter becomes thicker and older or increased input of isotopically evolved terrigenous material from erosion of the nearby arc and its basement.

The results of this study, in addition to supporting a significant role of crustal thickness on the variable chemical and isotopic

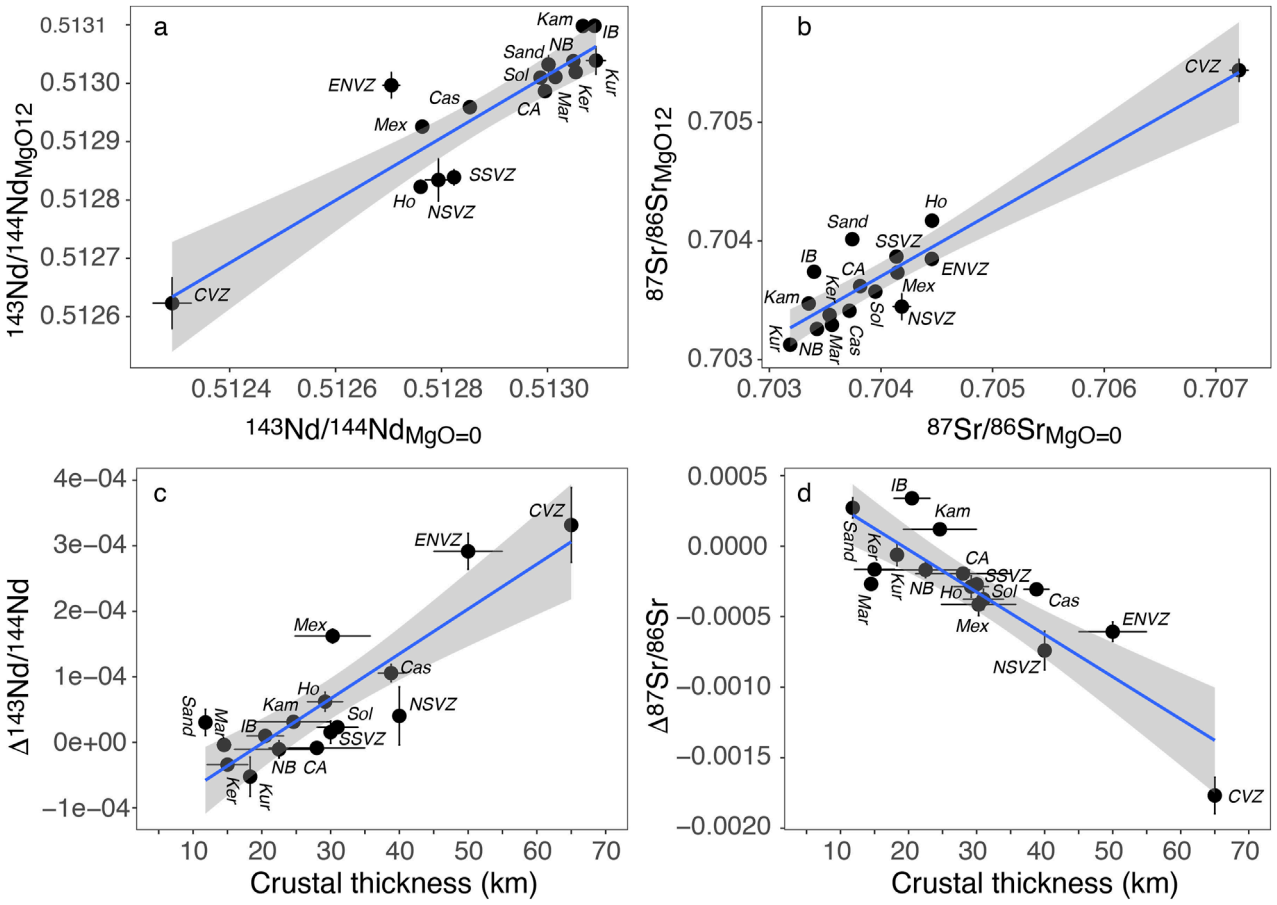

FIGURE 7
Plots of the correlations between $^{143}Nd/^{144}Nd$ at MgO = 12 wt% and $^{143}Nd/^{144}Nd$ at MgO = 0 wt% **(a)**, $^{87}Sr/^{86}Sr$ at MgO = 12 wt% and $^{87}Sr/^{86}Sr$ at MgO = 0 wt% **(b)**, crustal thickness and the $\Delta^{143}Nd/^{144}Nd$ **(c)**, and crustal thickness and $\Delta^{87}Sr/^{86}Sr$ **(d)**. $\Delta^{143}Nd/^{144}Nd$ and $\Delta^{87}Sr/^{86}Sr$ are the differences between $^{143}Nd/^{144}Nd$ and $^{87}Sr/^{86}Sr$ at 12 and 0 wt% MgO, respectively, calculated from the linear regressions of each arc in the $^{143}Nd/^{144}Nd$ and $^{87}Sr/^{86}Sr$ spaces. Gray envelopes are 1SD uncertainties for the regressions. Abbreviations as in Figure 2.

compositions of arc magmas both during crustal differentiation (Chiaradia, 2014; 2015) and, possibly, at their mantle source (Turner and Langmuir, 2015a; 2015b), are consistent with views of post-Archean, subduction-related crustal growth as a continuous process characterized by increasing thickness, SiO_2, and isotopically evolved compositions over time (Dhuime et al., 2015; Reimink et al., 2023), of which thin–intermediate and variably thick recent arcs could be a present-day snapshot.

Data availability statement

The datasets presented in this study can be found in online repositories. The names of the repository/repositories and accession number(s) can be found in the article/Supplementary Material.

Author contributions

MC: Conceptualization, Data curation, Formal Analysis, Funding acquisition, Investigation, Methodology, Project administration, Resources, Software, Supervision, Validation, Visualization, Writing – original draft, Writing – review and editing.

Funding

The author(s) declare that financial support was received for the research and/or publication of this article. The present study was supported by the Swiss National Science Foundation N. 200021_169032 (MC).

Conflict of interest

The authors declare that the research was conducted in the absence of any commercial or financial relationships that could be construed as a potential conflict of interest.

The author(s) declared that they were an editorial board member of Frontiers, at the time of submission. This

had no impact on the peer review process and the final decision.

Generative AI statement

The author(s) declare that no Generative AI was used in the creation of this manuscript.

Any alternative text (alt text) provided alongside figures in this article has been generated by Frontiers with the support of artificial intelligence and reasonable efforts have been made to ensure accuracy, including review by the authors wherever possible. If you identify any issues, please contact us.

Publisher's note

Supplementary material

The Supplementary Material for this article can be found online at: https://www.frontiersin.org/articles/10.3389/feart.2025.1690397/full#supplementary-material

References

Alasino, P. H., Paterson, S. R., Kirsch, M., and Larrovere, M. A. (2022). The role of crustal thickness on magma composition in arcs: an example from the pre-Andean, South American Cordillera. *Gondwana Res.* 106, 191–210. doi:10.1016/j.gr.2022.01.009

Annen, C., Blundy, J. D., and Sparks, R. S. J. (2006). The genesis of intermediate and silicic magmas in deep crustal hot zones. *J. Petrology* 47, 505–539. doi:10.1093/petrology/egi084

Bellver-Baca, M. T., Chiaradia, M., Beate, B., Beguelin, P., Deriaz, B., Mendez-Chazarra, N., et al. (2020). Geochemical evolution of the Quaternary chachimbiro volcanic complex (frontal volcanic arc of Ecuador). *Lithos* 356–357, 105237. doi:10.1016/j.lithos.2019.105237

Belousova, E. A., Kostitsyn, Y. A., Griffin, W. L., Begg, G. C., O'Reilly, S. Y., and Pearson, N. J. (2010). The growth of the Continental crust: constraints from zircon Hf-isotope data. *Lithos* 119, 457–466. doi:10.1016/j.lithos.2010.07.024

Cashman, K. V., Sparks, R. S. J., and Blundy, J. D. (2017). Vertically extensive and unstable magmatic systems: a unified view of igneous processes. *Science* 355, eaag3055. doi:10.1126/science.aag3055

Chiaradia, M. (2009). Adakite-like magmas from fractional crystallization and melting-assimilation of mafic lower crust (eocene macuchi arc, Western Cordillera, Ecuador). *Chem. Geol.* 265, 468–487. doi:10.1016/j.chemgeo.2009.05.014

Chiaradia, M. (2014). Copper enrichment in arc magmas controlled by overriding plate thickness. *Nat. Geosci.* 7, 43–46. doi:10.1038/ngeo2028

Chiaradia, M. (2015). Crustal thickness control on Sr/Y signatures of recent arc magmas: an Earth scale perspective. *Sci. Rep.* 5, 8115. doi:10.1038/srep08115

Chiaradia, M. (2021). Zinc systematics quantify crustal thickness control on fractionating assemblages of arc magmas. *Sci. Rep.* 11, 14667. doi:10.1038/s41598-021-94290-6

Chiaradia, M., and Fontboté, L. (2002). Lead isotope systematics of Late Cretaceous – tertiary andean arc magmas and associated ores between 8°N and 40°S: evidence for latitudinal mantle heterogeneity beneath the andes. *Terra nova.* 14, 337–342. doi:10.1046/j.1365-3121.2002.00426.x

Chiaradia, M., Müntener, O., and Beate, B. (2011). Enriched basaltic andesites from mid-crustal fractional crystallization, recharge, and assimilation (pilavo volcano, Western Cordillera of Ecuador). *J. Petrology* 52, 1107–1141. doi:10.1093/petrology/egr020

Chiaradia, M., Bellver-Baca, M. T., Valverde, V., and Spikings, R. (2021). Geochemical and isotopic variations in a frontal arc volcanic cluster (chachimbiro-pulumbura-pilavo-yanaurcu, Ecuador). *Chem. Geol.* 574, 120240. doi:10.1016/j.chemgeo.2021.120240

Davidson, J. P., Harmon, R. S., and Wörner, G. (1991). "The source of central Andean magmas; some considerations," in *Andean magmatism and its tectonic setting*. Editors R. S. Harmon, and C. W. Rapela (Boulder, CO: The Geological Society of America Inc.). doi:10.1130/SPE265-p233

DePaolo, D. J. (1981). Trace element and isotopic effects of combined wallrock assimilation and fractional crystallization. *Earth Planet. Sci. Lett.* 53, 189–202. doi:10.1016/0012-821X(81)90153-9

Dhuime, B., Wuestefeld, A., and Hawkesworth, C. J. (2015). Emergence of modern Continental crust about 3 billion years ago. *Nat. Geosci.* 8, 552–555. doi:10.1038/ngeo2466

Elliott, T., Plank, T., Zindler, A., White, W., and Bourdon, B. (1997). Element transport from slab to volcanic front at the mariana arc. *J. Geophys. Res. Solid Earth* 102, 14991–15019. doi:10.1029/97JB00788

Ewart, A., Collerson, K. D., Regelous, M., Wendt, J. I., and Niu, Y. (1998). Geochemical evolution within the tonga–kermadec–lau Arc–back-Arc systems: the role of varying mantle wedge composition in space and time. *J. Petrology* 39, 331–368. doi:10.1093/petroj/39.3.331

Farner, M. J., and Lee, C.-T. A. (2017). Effects of crustal thickness on magmatic differentiation in subduction zone volcanism: a global study. *Earth Planet. Sci. Lett.* 470, 96–107. doi:10.1016/j.epsl.2017.04.025

Goss, A. R., and Kay, S. M. (2006). Steep REE patterns and enriched Pb isotopes in southern Central American arc magmas: evidence for forearc subduction erosion? *Geochem. Geophys. Geosystems* 7. doi:10.1029/2005GC001163

Hagen-Peter, G., and Cottle, J. (2018). Evaluating the relative roles of crustal growth *versus* reworking through Continental arc magmatism: a case study from the ross orogen, Antarctica. *Gondwana Res.* 55, 153–166. doi:10.1016/j.gr.2017.11.006

Harmon, R. S., Barreiro, B. A., Moorbath, S., Hoefs, J., Francis, P. W., Thorpe, R. S., et al. (1984). Regional O-Sr-and Pb-isotope relationships in late Cenozoic calc-alkaline lavas of the andean Cordillera. *J. Geol. Soc.* 141, 803–822. doi:10.1144/gsjgs.141.5.0803

Hegner, E., and Smith, I. E. M. (1992). Isotopic compositions of late Cenozoic volcanics from southeast Papua New Guinea: evidence for multi-component sources in arc and rift environments. *Chem. Geol.* 97, 233–249. doi:10.1016/0009-2541(92)90078-J

Hildreth, W., and Moorbath, S. (1988). Crustal contributions to arc magmatism in the andes of central Chile. *Contr. Mineral. Petrol.* 98, 455–489. doi:10.1007/BF00372365

James, D. E. (1982). A combined O, Sr, Nd, and Pb isotopic and trace element study of crustal contamination in central Andean lavas, I. Local geochemical variations. *Earth Planet. Sci. Lett.* 57, 47–62. doi:10.1016/0012-821X(82)90172-8

James, D. E. (1984). "Quantitative models for crustal contamination in the central and northern andes," in *Andean magmatism: Chemical and isotopic constraints*. Editors R. S. Harmon, and B. A. Barreiro (Boston, MA: Birkhäuser), 124–138. doi:10.1007/978-1-4684-7335-3_9

James, D. E., and Murcia, L. A. (1984). Crustal contamination in northern Andean volcanics. *J. Geol. Soc.* 141, 823–830. doi:10.1144/gsjgs.141.5.0823

Jenner, F. E. (2017). Cumulate causes for the low contents of sulfide-loving elements in the Continental crust. *Nat. Geosci.* 10, 524–529. doi:10.1038/ngeo2965

Jicha, B. R., and Kay, S. M. (2018). Quantifying arc migration and the role of forearc subduction erosion in the central aleutians. *J. Volcanol. Geotherm. Res.* 360, 84–99. doi:10.1016/j.jvolgeores.2018.06.016

Kay, S. M., Godoy, E., and Kurtz, A. (2005). Episodic arc migration, crustal thickening, subduction erosion, and magmatism in the south-central andes. *GSA Bull.* 117, 67–88. doi:10.1130/B25431.1

Kay, S. M., Mpodozis, C., and Gardeweg, M. (2014). "Magma sources and tectonic setting of Central andean andesites (25.5–28°S) related to crustal thickening, forearc subduction erosion and delamination," in *Orogenic Andesites and Crustal Growth*, ed. A. Gómez-Tuena, S. M. Straub, and G. F. Zellmer (Bath: The Geological Society of London), 385, 303–334. doi:10.1144/SP385.11

Kelemen, P. B., Hanghoj, K., and Greene, A. R. (2004). "One view of the geochemistry of subduction-related magmatic arcs, with an emphasis on primitive andesite and lower crust," in *Treatise on geochemistry*. Editors H. D. Holland, and K. K. Turekian (Amsterdam), 593–659. Elsevier, Amsterdam. 3.

Kemp, A. I. S., Hawkesworth, C. J., Foster, G. L., Paterson, B. A., Woodhead, J. D., Hergt, J. M., et al. (2007). Magmatic and crustal differentiation history of granitic rocks from Hf-O isotopes in zircon. *Science* 315, 980–983. doi:10.1126/science.1136154

Koch, C. D., Delph, J., Beck, S. L., Lynner, C., Ruiz, M., Hernandez, S., et al. (2021). Crustal thickness and magma storage beneath the Ecuadorian arc. *J. S. Am. Earth Sci.* 110, 103331. doi:10.1016/j.jsames.2021.103331

Large, S. J. E., Nathwani, C. L., Wilkinson, J. J., Knott, T. R., Tapster, S. R., and Buret, Y. (2024). Tectonic and crustal processes drive multi-million year arc magma evolution leading up to porphyry copper deposit formation in central Chile. *J. Petrology* 65, egae023. doi:10.1093/petrology/egae023

Lee, C.-T. A., and Tang, M. (2020). How to make porphyry copper deposits. *Earth Planet. Sci. Lett.* 529, 115868. doi:10.1016/j.epsl.2019.115868

Lee, C.-T. A., Luffi, P., Chin, E. J., Bouchet, R., Dasgupta, R., Morton, D. M., et al. (2012). Copper systematics in arc magmas and implications for crust-mantle differentiation. *Science* 336, 64–68. doi:10.1126/science.1217313

Li, H., Hermann, J., and Zhang, L. (2022). Melting of subducted slab dictates trace element recycling in global arcs. *Sci. Adv.* 8, eabh2166. doi:10.1126/sciadv.abh2166

Loucks, R. R. (2021). Deep entrapment of buoyant magmas by orogenic tectonic stress: its role in producing Continental crust, adakites, and porphyry copper deposits. *Earth-Science Rev.* 220, 103744. doi:10.1016/j.earscirev.2021.103744

Mamani, M., Tassara, A., and Wörner, G. (2008). Composition and structural control of crustal domains in the central andes. *Geochem. Geophys. Geosystems* 9. doi:10.1029/2007GC001925

Mamberti, M., Lapierre, H., Bosch, D., Jaillard, E., Ethien, R., Hernandez, J., et al. (2003). Accreted fragments of the Late Cretaceous Caribbean–Colombian Plateau in Ecuador. *Lithos* 66, 173–199. doi:10.1016/S0024-4937(02)00218-9

Miller, C. F., and Wark, D. A. (2008). Supervolcanoes and their explosive supereruptions. *Elements* 4, 11–15. doi:10.2113/GSELEMENTS.4.1.11

Nandedkar, R. H., Ulmer, P., and Müntener, O. (2014). Fractional crystallization of primitive, hydrous arc magmas: an experimental study at 0.7 GPa. *Contrib. Mineral. Petrol* 167, 1–27. doi:10.1007/s00410-014-1015-5

Nielsen, S. G., and Marschall, H. R. (2017). Geochemical evidence for mélange melting in global arcs. *Sci. Adv.* 3, e1602402. doi:10.1126/sciadv.1602402

Plank, T. (2005). Constraints from thorium/lanthanum on sediment recycling at subduction zones and the evolution of the continents. *J. Petrology* 46, 921–944. doi:10.1093/petrology/egi005

Profeta, L., Ducea, M. N., Chapman, J. B., Paterson, S. R., Gonzales, S. M. H., Kirsch, M., et al. (2015). Quantifying crustal thickness over time in magmatic arcs. *Sci. Rep.* 5, 17786. doi:10.1038/srep17786

R Core Team (2013). *R: a language and environment for statistical computing*. Vienna, Austria: R Foundation for Statistical Computing. Available online at: http://www.R-project.org/.

Reimink, J. R., Davies, J. H. F. L., Moyen, J.-F., and Pearson, D. G. (2023). A whole-lithosphere view of Continental growth. *Geochem. Perspect. Lett.* 26, 45–49. doi:10.7185/geochemlet.2324

Reubi, O., and Blundy, J. (2009). A dearth of intermediate melts at subduction zone volcanoes and the petrogenesis of arc andesites. *Nature* 461, 1269–1273. doi:10.1038/nature08510

Rudnick, R. L., and Gao, S. (2005). "Composition of the Continental crust," in *Treatise on geochemistry - the crust* (Amsterdam: Elsevier), 1–64.

Shuto, K., Ishimoto, H., Hirahara, Y., Sato, M., Matsui, K., Fujibayashi, N., et al. (2006). Geochemical secular variation of magma source during early to middle Miocene time in the Niigata area, NE Japan: asthenospheric mantle upwelling during back-arc basin opening. *Lithos* 86, 1–33. doi:10.1016/j.lithos.2005.06.001

Sillitoe, R. H. (2010). Porphyry copper systems. *Econ. Geol.* 105, 3–41. doi:10.2113/gsecongeo.105.1.3

Sisson, T. W., Ratajeski, K., Hankins, W. B., and Glazner, A. F. (2005). Voluminous granitic magmas from common basaltic sources. *Contrib. Mineral. Petrol* 148, 635–661. doi:10.1007/s00410-004-0632-9

Stern, C. R. (2011). Subduction erosion: rates, mechanisms, and its role in arc magmatism and the evolution of the Continental crust and mantle. *Gondwana Res.* 20, 284–308. doi:10.1016/j.gr.2011.03.006

Takanashi, K., Kakihara, Y., Ishimoto, H., and Shuto, K. (2012). Melting of crustal rocks as a possible origin for middle Miocene to Quaternary rhyolites of northeast Hokkaido, Japan: constraints from Sr and Nd isotopes and major- and trace-element chemistry. *J. Volcanol. Geotherm. Res.* 221–222, 52–70. doi:10.1016/j.jvolgeores.2011.11.008

Tassara, A., and Echaurren, A. (2012). Anatomy of the Andean subduction zone: three-dimensional density model upgraded and compared against global-scale models. *Geophys J. Int.* 189, 161–168. doi:10.1111/j.1365-246X.2012.05397.x

Turner, S. J., and Langmuir, C. H. (2015a). The global chemical systematics of arc front stratovolcanoes: evaluating the role of crustal processes. *Earth Planet. Sci. Lett.* 422, 182–193. doi:10.1016/j.epsl.2015.03.056

Turner, S. J., and Langmuir, C. H. (2015b). What processes control the chemical compositions of arc front stratovolcanoes? *Geochem. Geophys. Geosystems* 16, 1865–1893. doi:10.1002/2014GC005633

Wallace, P. J. (2005). Volatiles in subduction zone magmas: concentrations and fluxes based on melt inclusion and volcanic gas data. *J. Volcanol. Geotherm. Res.* 140, 217–240. doi:10.1016/j.jvolgeores.2004.07.023

Wieser, P. E., Turner, S. J., Mather, T. A., Pyle, D. M., Savov, I. P., and Orozco, G. (2019). New constraints from central Chile on the origins of enriched Continental compositions in thick-crusted arc magmas. *Geochimica Cosmochimica Acta* 267, 51–74. doi:10.1016/j.gca.2019.09.008

Workman, R. K., and Hart, S. R. (2005). Major and trace element composition of the depleted MORB mantle (DMM). *Earth Planet. Sci. Lett.* 231, 53–72. doi:10.1016/j.epsl.2004.12.005

Zellmer, G. F., Iizuka, Y., and Straub, S. M. (2024). Origin of crystals in mafic to intermediate magmas from circum-pacific Continental arcs: transcrustal magmatic systems *versus* transcrustal plutonic systems. *J. Petrology* 65, egae013. doi:10.1093/petrology/egae013

Zhang, Y., Gazel, E., Gaetani, G. A., and Klein, F. (2021). Serpentinite-derived slab fluids control the oxidation state of the subarc mantle. *Sci. Adv.* 7, eabj2515. doi:10.1126/sciadv.abj2515

Zhao, S.-Y., Yang, A. Y., Langmuir, C. H., and Zhao, T.-P. (2022). Oxidized primary arc magmas: constraints from Cu/Zr systematics in global arc volcanics. *Sci. Adv.* 8, eabk0718. doi:10.1126/sciadv.abk0718